6-22-2005

On Multiscale Approaches to 3-Dimensional Modeling of Morphogenesis

Rajiv Chaturvedi

Chengbang Huang

Bogdan Kazmierczak

T. Schneider

Jesus A. Izaguirre

See next page for additional authors

On Multiscale Approaches to Three-Dimensional Modeling of Morphogenesis

By

R. Chaturvedi[1], C. Huang[2], B. Kazmierczak[1], T. Schneider[2], J. A. Izaguirre[2], T. Glimm[3],

H. G. E. Hentschel[3], S. A. Newman[4], J. A. Glazier[5], M. Alber[1,†]

† Author for correspondence: M. S. Alber, 255 Hurley Building, University of Notre Dame, Notre Dame, IN 46556-5670. email: malber@nd.edu, web: http://www.nd.edu/~malber/ , phone: (574) 631 8371, fax: (574) 631-6579.

[1] Department of Mathematics and Center for the Study of Biocomplexity, University of Notre Dame, Notre Dame, IN 46556-5670.

[2] Department of Computer Science and Engineering, University of Notre Dame, Notre Dame, IN 46556-5670.

[3] Department of Physics, Emory University, Atlanta, GA 30322

[4] Department of Cell Biology & Anatomy, New York Medical College, Vallaha, NY

[5] Biocomplexity Institute and Department of Physics, Indiana University, 727 East 3rd Street, Swain Hall West 159, Bloomington, IN 47405-7105.

Abstract

In this paper we present the foundation of a unified, object-oriented, three-dimensional (*3D*) biomodeling environment, which allows us to integrate multiple submodels at scales from subcellular to tissues and organs. Our current implementation combines a modified discrete model from statistical mechanics, the Cellular Potts Model (*CPM*), with a continuum reaction-diffusion (*RD*) model and a state automaton with well-defined conditions for cell differentiation transitions to model genetic regulation. This environment allows us to rapidly and compactly create computational models of a class of complex developmental phenomena. To illustrate model development, we simulate a simplified version of the formation of the skeletal pattern in a growing embryonic vertebrate limb.

Keywords:

Computational biology, systems biology, morphogenesis, organogenesis, cell dynamics, Cellular Potts Model, reaction-diffusion, vertebrate limb, multiscale models, pattern formation, Monte Carlo simulations, hybrid continuous-discrete models.

Table of Contents

1 Introduction

New information about the many specific biological mechanisms acting at various scales in multicellular organisms is inspiring increasing collaboration between experimentalists and modelers to build predictive simulations of complex biological phenomena. Such simulations must describe the interactions among the various natural biological scales (molecular, subcellular, cellular and supracellular). While individual organisms and organs have very different structures and behaviors, many of the underlying interactions and components are common. Thus we can greatly reduce the burden of simulation by building a software framework that includes the fundamental mechanisms and objects, and allows us to specify them and their interactions in a compact way.

The paper adopts this approach to provide a three-dimensional (*3D*) environment for modeling *morphogenesis*, the pattern of structural development of an organism or its organs, during vertebrate embryo development. A version of the code is available as the CompuCell3D project on the web[1]. Morphogenesis involves differentiation, growth, death and migration of cells, as well as changes in the shapes of cells and tissues and the secretion and absorption of extracellular materials.

Figure 1 shows the hierarchy of scales our computational environment includes. Information usually flows from finer to coarser scales, but can flow between any pair of submodels. For example, cells secrete peptide signaling factors under certain conditions, and such factors may act as *morphogens* which modify the type of the secreting cell or its neighbors. In this case, a supercellular diffusant affects a subcellular differentiation state. Section 2 justifies our modeling approach. Section 3 provides biological details on

[1] http://www.nd.edu/~lcls/compucell

phenomena occurring at multiple scales and their interactions. We then provide details on each of the blocks in Figure 1: Section 4.1 describes the cell-scale submodel, the Cellular Potts Model (*CPM*), which is the core module of the computational environment. Sections 4.2 and 4.3 describe molecular-scale submodels, Section 4.4 a phenomenological, subcellular submodel of the Gene Regulatory Network and Sections 4.5 and 4.6 the complete organ-scale model. Our implementation of a computational environment for morphogenesis allows us to construct computer models within the environment, enabling us to study the parameter-rich complexity of the complete biological models that result from webs of interactions between the components of the hybrid model**.** The software implementation of models requires specification of: (i) the interfaces between interacting submodels, and (ii) a simulation protocol that specifies the spatial and temporal order in which the component submodels execute.

What justifies a multiscale modeling approach? Why is the cell the natural level of detail to begin with? Macroscopic models, such as Physiome[2], which treat tissues as continuous substances with bulk mechanical properties, reproduce many biological phenomena but fail when biological structure develops and functions at the cell scale. Often direct, cell-level implementations reproduce phenomena which we see in experiments but which the continuum model misses. However, continuum models to describe acellular materials like bone, extracellular matrix (*ECM*), fluids and diffusing chemicals are much less computationally costly than cell development models. Molecular and subcellular models like V-cell[3] or BioSym[4] provide detail on aspects of subcellular processes but often cannot describe even one complete cell, let alone many cells acting in

[2] http://www.physiome.org
[3] http://www.ibiblio.org/virtualcell/index.htm
[4] http://www.accelrys.com/about/msi.html

concert. In addition, even a hypothetical 'perfect' cell replica (which is probably computationally infeasible) would not provide an understanding of how cells and organisms function. Instead, reaction kinetics can efficiently and realistically model cell differentiation and metabolism. A cell-level model like the CPM can simulate 10^5 - 10^6 cells on a single processor, making whole-organism simulations practical on parallel computers. When appropriate, cell-level models can supply parameters to and interface with continuum models, accept parameters from microscopic models or use phenomenological models of subcellular properties. In this respect, biological modeling is easier than materials modeling, which lacks the natural mesoscopic level of the cell to interpolate between molecule and continuum.

As an example of such model descriptions, we use the general biological concept that interactions of cells *via* gene products (*i.e.*, molecules synthesized by gene transcription and translation, and their derivatives) generate biologically significant patterning instabilities that we can describe mathematically and implement computationally [1 – 8]. Gene products may reside inside a cell, on the cell surface, or cells may secrete them. Secreted gene products may remain at their secretion location or diffuse or advect, possibly over long distances. In this paper we neglect the advection of gene products and consider only their diffusion (see Section 3 for a justification); we do include motion of cells and their surrounding medium.

As an example of implementing a specific, though simplified, developmental simulation within our computational environment, we construct a model of the dramatic patterning of developing cartilage (*i.e.*, spatiotemporal *chondrogenesis*) which occurs in

the pre-differentiated mass of mesenchymal cells during the embryonic growth of the early-stage avian limb bud (see Figure 2, day 4).

The developing vertebrate limb progressively generates a sequence of increasing numbers of cartilage elements from the body-wall outwards (*proximo-distally*) (see Figure 2). In a forelimb, this sequence is (i) humerus, (ii) radius and ulna, (iii) carpals and metacarpals, and (iv) digits. The hindlimb displays a similar pattern: (i) femur, (ii) tibia and fibula, (iii) tarsals and metatarsals, and (iv) digits. Independent of limb type, element (i) is the *stylopod*, element set (ii) the *zeugopod*, and element sets (iii) and (iv) the *autopod*.

The developing limb presents a number of distinct problems in growth and patterning. How does the genetic program interact with generic, dynamic physical and chemical mechanisms to form an organ? What is the relative contribution of local and long-range signaling? What are specific factors that result in abnormal growth? To succeed, our model must reproduce both normal and abnormal development, and should suggest mechanisms for observed pathologies.

To answer these questions, we need to develop a predictive model. Distinguishing between experimental biological, mathematical and computational models clarifies model building. Limbs display a great variety of structures and functions of varying degrees of organizational complexity. For example, the adaptations of limbs can range from the flipper of a dolphin, to the wings of a bird, the hoofed feet of horses, and the dexterous forelimbs of humans. We need to organize our biological study in a manner that exemplifies the underlying unity of structure, function and organizational principles, while allowing elaborations to explain specific differences. Continuing with our limb

example, the chicken is a widely studied *experimental model* (both *in-vivo* and *in-vitro*) of vertebrate limb development. Computational biology's (*in-silico*) first step is to develop a *biological model* describing the observed experimental behaviors. Diagrams of biochemical pathways or cell migration are examples of such biological models. We then construct a *mathematical model* to quantitatively express the phenomena the biological model describes. The mathematical model consists either of sets of differential equations or algorithms, or a combination of the two. We need idealizations to simplify the observed phenomena at this step, but the mathematical model must be rich enough to capture the range of phenomena we wish to predict.

Even idealizations of the simplest organisms are generally too complex to permit us to solve the mathematical models analytically; hence we translate the mathematical model into a *computer model* or *simulation*. The commonality of biological processes allows us to build a modeling framework which allows simple, compact and efficient implementation of mathematical models as computational models. We use the modeling framework to build a composite model of the complex web of interactions of the mathematical model, using submodels representing different scales. To be *extensible* and reusable (*i.e.,* able to accommodate model elaborations and changes without requiring rewriting of old code) the computational environment must be *modular* (*i.e.,* constructed from well-defined, independent components), with well-defined interfaces through which the various submodels interact, allowing us to construct new objects and submodels, which is essential because of the current rapid growth in our knowledge of cellular and subcellular mechanisms. Neuron[5] and Physiome[6] are examples of such frameworks.

[5] http://www.neuron.yale.edu/neuron
[6] http://www.physiome.org

Multiscale, experimentally-motivated simulations have successfully used the CPM to reproduce morphological phenomena in the cellular slime mold *Dictyostelium discoideum* [9, 10], vertebrate neurulation [11] and convergent extension [12]. Chaturvedi *et al.* [13] and later Izaguirre *et al.* [14] described a simplified, 2D environment, *CompuCell*, which integrated discrete and continuum models of biological mechanisms. A highly-simplified, sample simulation in this environment reproduced the proximo-distal increase in the number of skeletal elements in the developing avian limb. This paper emphasizes the modeling issues involved in extending the software framework to 3D, and implements a more experimentally accurate sample simulation realizing a more biologically-motivated model of limb development [3]. Using this model, we simulate two pathological cases of limb development in addition to normal development.

2 Modeling Organogenesis

Organogenesis, an example of morphogenesis, is the development of organs in living organisms. Our software framework for organogenesis includes three major submodels: the discrete stochastic CPM for cell dynamics, continuum Reaction-Diffusion (*RD*) partial differential equations (*PDE*s) for morphogen production and diffusion, and a Type-change model for genetic regulation.

Traditionally, models dealing with organogenesis, *e.g.*, the 2D continuum model of chicken limb development in Hentschel *et al*. [3], treat both cells and morphogens as continuous fields. Continuum models work well for diffusing chemicals, whose distribution varies over distances much larger than a cell diameter. Modeling the motion of individual morphogen molecules would require a tremendous amount of computer

time. By treating their concentrations as continua, we take advantage of computationally efficient optimal standard numeric schemes for RD PDEs for secreted morphogens. Models at the cell-scale require representation of individual cells, which undergo changes in shape and assocation with other cells and ECM in forming different kinds of tissues (epithelia, cartilage, *etc*.) [3]. Cells also move considerable distances during organogenesis, so treating them as a continuum field would require numerical solutions of advection PDEs, which are computationally costly and numerically unstable.

Organogenesis depends on 3D cell rearrangement. Although 2D simulations provide helpful qualitative insights using limited computer resources [13, 14], understanding symmetries and symmetry breaking during organogenesis requires 3D modeling and simulation; 3D mathematical and physical models differ qualitatively from those in 2D.

For example, in the CPM part of our chick-limb model, a third dimension allows cells to move around barriers, relaxing 2D constraints on producing specific cell condensation-dependent tissue structures (*e.g.*, the nodular and bar-like precartilage primordia involved in skeletogenesis). In the RD part of the chick-limb model the diffusing morphogens serve as both *inductive* signals (*i.e.*, altering cell type) and *haptotactic* signals (*i.e.*, inducing preferential cell movement up a gradient of an insoluble ECM molecule; see below). A requirement specific to the 3D RD submodel is that the morphogen patterns must display simultaneous spot-like and stripe-like behavior (Section 4.2.2). In this paper we use a biologically-motivated RD model which Hentschel *et al*. [3] proposed and solved in 2D, where simultaneous spot-stripe behavior was not required. These RD equations in 3D require additional stabilizing cubic terms, making them structurally more complex than the 2D equations (for details, see Section 4.2).

3 Biological Background: Multiple Scales in Limb Organogenesis

Cell condensation is a critical stage in chondrogenesis (Figure 2 shows the stages of chondrogenesis in the chicken limb). Why and how do the initially dispersed *mesenchymal* cells cluster at specific locations within the paddle-shaped tissue *mesoblast* that emerges from the body wall, and how do they form the precartilage template for the limb skeleton? While genes specify the proteins (both intracellular and secreted into extracellular space) necessary for morphogenesis, the genes do not, by themselves, specify the distribution of these proteins or their physical effects. *Generic* physical mechanisms complement and enable the *genetic* mechanisms. Generic mechanisms (in the context of tissue mechanics) are physical mechanisms common to both living and nonliving viscoelastic or excitable materials, which translate gene expression into mechanical behavior [16] as well as dynamic chemical processes that regulate the state of chemical reactors, including cells [17]. The regulation of gene expression is one important aspect of development, but a full description of development requires incorporation of the thermodynamics and mechanics of condensed matter, as well as the pattern-forming instabilities of excitable media at the scales of tissues, organs and organisms.

Figure 3 schematically represents the major axes and the progress of chondrogenic patterning of a developing vertebrate forelimb. The humerus has already differentiated (black); the radius and ulna are forming (medium gray). The wrist bones and digits are still to form.

Limb formation in chicken and other vertebrates starts with a mesoblast consisting of two main populations of pre-differentiated mesenchymal cells, precartilage

and pre-muscle cells (reviewed in [18]). To start with, precartilage cells pack loosely in the mesoblast. Subsequently they divide and change position under various influences, finally condensing into patterns that prefigure the bones. As the limb bud elongates, subpopulations of precartilage cells successively condense and differentiate into *chondrocytes*, beginning in the *proximal* (nearer to body) region and eventually extending to the *distal* (far from body) region of the growing limb bud. The distal-most region (the *Apical Zone*) progressively shortens in the proximo-distal direction but remains in the pre-differentiated mesenchymal state until skeletal development ends. A sheet of tightly attached cells called *ectoderm* sheathes the mesoblast. The narrow protrusion of the ectoderm that runs in an antero-posterior direction along the distal tip of the limb bud is the *Apical Ectodermal Ridge* (AER). An apically-localized source of fibroblast growth factors (FGFs) (see below), provided under normal circumstances by the AER,, is necessary for proximo-distal development of the skeleton. The initial precartilage mesenchymal cell *type* differentiates into other cell types under the influence of various signals. At sites of condensation, cells differentiate into cartilage; at other sites they differentiate into *connective tissue* (tendon, muscle-associated supporting tissue and, in certain species, interdigital webs) or undergo *apoptosis* (programmed cell death). The muscle cells of the limb differentiate from a separate population of limb mesenchymal cells (see [18]).

Key mechanisms in chondrogenic patterning include cell *motility*, and *adhesion* between different types of cells [19] and between cells and the ECM. ECM components are non-diffusing secreted proteins and other polymeric molecules which act as scaffolds

or attachment substrata (*e.g.*, fibronectin). The ECM also provides a medium through which morphogens diffuse.

Secreted components have various dynamics and effects. Experiments on the initiation and arrangement of individual skeletal elements in chicken and mouse suggest that the secreted morphogens TGF-β, FGF-2 and FGF-8 are key molecules (see Hentschel *et al*. 2004 [3] for a review). Experiments [28, 29, 40, 41] and simulations [5, 8] of disk-shaped, high-density (micromass) cultures of limb precartilage mesenchyme show the importance of fibronectin in chondrogenic pattern formation. *Haptotaxis* (cell movement up or down gradients either of bound chemicals or mechanical properties in the substrate) of cells in response to fibronectin produces various chondrogenic patterns. Fibronectin is a large molecule, which does not diffuse like TGF-β, although it can spread from its point of production by other mechanisms [42]. In our model we consider two main secreted components—TGF-β, which diffuses through the mesoblast (inclusive of cells and ECM), and fibronectin, which accumulates at sites of secretion. The *ground substance* of the mesoblast is a dilute aqueous gel containing the *glycosaminoglycan* (tissue polysaccharide) hyaluronan. We assume that this gel supports the cells and provides a medium for diffusion of TGF-β and a hypothesized inibitor of chondrogenesis (see below) and for accumulation of fibronectin. This gel and the cells it supports both move as the limb grows. We assume that this motion is very slow compared to the morphogens' diffusion speed. This assumption allows us to neglect advection of morphogens by the ECM.

We assume that TGF-β triggers the precartilage mesenchymal cells' differentiation into cells capable of producing fibronectin [20]. Cells respond to

fibronectin by undergoing *haptotaxis*, *i.e.*, cells adhere to, and therefore move more slowly in the presence of, fibronectin. Due to the diffusive nature of cell movement, the net result is motion up gradients of fibronectin. In addition, TGF-β upregulates production of the cell-surface molecule N-cadherin which regulates cell-cell adhesivity [21, 22].

TGF-β can diffuse through the mesoblast. It is positively autoregulatory [23, 24]. Together with a hypothesized inhibitor of its action or its downstream effectors [27], it can potentially form patterns via reaction-diffusion [24, 25, 26, 27]. Since TGF-β also induces cells to produce fibronectin and upregulates cell-cell adhesivity, it recruits neighboring cells into chondrogenic condensations [27, 29].

We can think of the developing limb as containing three zones—the Apical Zone where only cell division takes place, the *Active Zone* where cells rearrange locally into precartilage condensations and the *Frozen Zone* in which condensations have differentiated into cartilage and no additional patterning takes place. Cell division continues in both Active and Frozen Zones [30]. Biologically, distance from the AER, perhaps, signaled by the concentrations of a subset of the FGFs, may define the zones [3]; however, for simplicity, we assume the zones *a priori*.

4 Physical and Mathematical Submodels and their Integration

We describe below specific physical and mathematical representations of key biological mechanisms operating at the various scales of our model. Table 1 summarizes the mechanisms and the corresponding submodels. For each mechanism a specific parameter controls the behavior of the corresponding submodel. Table 2 lists important mechanisms and their control parameters.

4.1 Modeling Cellular and Tissue Scales: the CPM Framework

Cell-scale processes are the basis for the complexity of highly evolved multicellular organisms, as well as colonies of unicellular ones. In multicellular organisms, ECM plays an important role (Section 3). We can model ECM components either at the scale of cells or smaller scales. In this paper we choose to model the ECM gel at the cell scale, and fibronectin at a finer scale.

Physics of cell sorting: Condensation requires sorting of similar types of cells into cell clusters. Steinberg disaggregated cells, re-mixed them randomly and found that they sorted into coherent clusters [31]. He proposed the Differential Adhesion Hypothesis (DAH), which states that cells adhere to each other with different strengths depending on their types. Cell sorting results from random motions of the cells that allow them to minimize their configuration energy; this phenomenon is analogous to the surface-tension-driven phase separation of two immiscible liquids. If cells of the same type adhere more strongly, they gradually cluster together, with less adhesive cells surrounding the more adhesive ones. Differential adhesion results from differences (controlled at the subcellular level) in the expression of adhesion molecules on cell membranes, which may vary both in quantity and identity.

Based on the physics of the DAH, we model adhesive phenomena as variations in cell-specific adhesivity at the cell level, rather than at the level of individual molecules and their interactions. Simple thermodynamics then accounts for the macroscopic behavior of cell mixtures at the scale of cell aggregation into tissues.

The Extended CPM Framework: The CPM, as originally proposed, provided a physical formalism for studying the implications of the DAH [1]. It is a generalization of the Ising

model, and shares the Ising model's core idea of modeling dynamics based on energy minimization under imposed fluctuations. As long as we can describe a process in terms of a real or effective potential energy, we can include it in the CPM framework by adding it to the other terms in the energy. We extend the original CPM framework to (i) model haptotaxis by adding an extra chemical potential term to the original CPM energy, (ii) include time variation in the adhesivity of cells, (iii) accommodate cell growth, and, (iv) provide a phenomenological mechanism for cell division (mitosis).

Modeling Living Cells and ECM (discrete representation on a grid): The CPM uses a lattice to describe cells. We associate an integer index to each lattice site (*voxel*) to identify the space a cell occupies at any instant (Figure 4). The value of the index at a lattice site (*i,j,k*) is σ if the site lies in cell σ. *Domains* (*i.e.*, collection of lattice sites with the same index) represent cells. Thus, we treat a cell as a set of discrete subcomponents that can rearrange to produce cell motion and shape changes. Figure 4 shows three cells and the ECM, which require four distinct indices.

We model ECM (liquid medium and solid substrates) as generalized cells with distinct indices, unless a specific component of the ECM requires more detailed modeling (*e.g.*, fibronectin, see below). Thus we can have advection of cells as well as ECM.

We model some cell behaviors on the lattice employed by the CPM, but others, which have different dynamics, require modeling outside the CPM framework. Growth and division are examples of cell behaviors that we describe on the CPM grid, but require additional dynamics or conditions. Cell differentiation requires modeling the Gene Regulatory Network, which controls the CPM parameters; it requires a separate, microscopic submodel and integration into the hybrid environment.

To model cell dynamics, the CPM uses an effective energy, *E. E* consists of true energies (*e.g.*, cell-cell adhesion) and terms that mimic energies (*e.g.*, the response of a cell to a chemotactic gradient). Cells evolve under strong damping. The dynamics penalizes disconnected domains of lattice sites with same index. Upadhyaya [32], Ouchi [46], and Marée [9] have used the CPM to reproduce the behavior of cell aggregates of different kinds in 2D and 3D.

Dynamics of cell rearrangement: In mixtures of liquid droplets, thermal fluctuations of the droplet surfaces cause diffusion (*Brownian motion*) leading to minimization of surface energy. We model membrane fluctuations as simple thermal fluctuations. The fluctuations drive the cells' configuration to a global energy minimum, rather than to one of the multiple local minima of energy that can coexist. We phenomenologically assume that an *effective temperature, T*, drives cell membrane fluctuations. *T* defines the size of the typical fluctuation. We implement fluctuations using the Metropolis algorithm for Monte-Carlo Boltzmann dynamics (see [1] and [8]). If a proposed change in lattice configuration (*i.e.*, a change in the indices associated with the voxels of the lattice) produces a change in effective energy, ΔE, we accept it with probability:

$$P(\Delta E) = 1, \Delta E \leq 0; \qquad P(\Delta E) = e^{-\Delta E / kT}, \Delta E > 0, \qquad (1)$$

where *k* is a constant converting *T* into units of energy.

E includes terms to describe each mechanism we have decided to include, *e.g.*,

$$E = E_{Contact} + E_{Volume} + E_{Chemical}. \qquad (2)$$

We describe each of these terms below.

Cell–cell adhesion: In Equation 2, E_{contact} phenomenologically describes the net adhesion/repulsion between two cell membranes. It is the product of the binding energy per unit area, $J_{\tau,\tau'}$, and the area of interaction of the two cells. In our model, $J_{\tau,\tau'}$ depends on the specific properties of the interacting cells.

$$E_{Contact} = \sum_{(i,j,k)(i',j',k')} J_{\tau(\sigma)\tau'(\sigma')}(1-\delta(\sigma(i,j,k),\sigma'(i',j',k'))), \qquad (3)$$

where the *Kronecker delta*, $\delta(\sigma,\sigma')=0$ if $\sigma\neq\sigma'$ and $\delta(\sigma,\sigma')=1$ if $\sigma=\sigma'$, ensures that only links between surface sites in different cells contribute to the cell adhesion energy. The adhesive interactions operate over a prescribed range around each lattice site. Figure 4 shows a fourth-nearest-neighbor interaction range. In 2D each lattice site has four nearest neighbors. In 3D the number of nearest neighbors is six.

Cell size and shape fluctuations: A cell of type τ has a prescribed *target volume* $v(\sigma,\tau)$ and *target surface area* $s(\sigma,\tau)$ corresponding to the averages for cell-type τ. The actual volume and surface area fluctuate around these target values, *e.g.*, due to changes in osmotic pressure, pseudopodal motion of cells, *etc.* Changes also result from growth and division of cells during morphogenesis. E_{volume} enforces these targets by exacting an energy penalty for deviations. E_{volume} depends on four model parameters: *volume elasticity*, λ, *target volume*, $v_{\text{target}}(\sigma,\tau)$, *membrane elasticity*, λ', and *target surface area*, $s_{\text{target}}(\sigma,\tau)$:

$$E_{volume} = \sum_{\text{all-cells}} \lambda_\sigma (v(\sigma,\tau) - v_{\text{target}}(\sigma,\tau))^2 + \sum_{\text{all-cells}} \lambda'_\sigma (s(\sigma,\tau) - s_{\text{target}}(\sigma,\tau))^2. \qquad (4)$$

Changing the ratio of $v^{2/3}{}_{\text{target}}(\sigma,\tau)$ to $s_{\text{target}}(\sigma,\tau)$ changes the rigidity or floppiness of the cell shape.

Chemotaxis and haptotaxis: In principle, cells can respond to both diffusible chemical signals and insoluble ECM molecules by moving along concentration gradients of these substances. Although chemotaxisis is readily accomodated within CompuCell3D, there is no evidence that the mesenchymal cells of the developing limb respond chemotactically to any of the molecules in our core genetic network. We therefore have not included chemotaxis in the simulations presented here. Haptotaxis requires a representation of an evolving, spatially-varying concentration field, and a mechanism linking the field to the framework for cell and tissue dynamics. The former depends on the particular ECM molecule (Sections 4.2 and 4.3). We denote the local concentration of the molecules in extracellular space by $C(\vec{x})$. An effective chemical potential, $\mu(\sigma)$ models haptotaxis, and the following term incorporates the effective chemical energy into the CPM energy formalism:

$$E_{chemical} = \mu(\sigma)C(\vec{x}). \qquad (5)$$

Cell Growth, Division and Cell Death: Equations 3, 4 and 5 used the energy formalism of the CPM to model certain cell behaviors. We also use the CPM lattice to model cell growth, division and death. Cell growth and death affect the CPM model parameters $v_{\text{target}}(\sigma,\tau)$ and $s(\sigma,\tau)$. We model cell growth by allowing the values of $v_{\text{target}}(\sigma,\tau)$ and $s(\sigma,\tau)$ to increase with time at a constant rate. Growth properties depend on cell type (Section 4.4).

We can model cell death simply by setting the cell's target volume to zero.

Cell division occurs when the cell reaches a fixed, type-dependent volume. We model division by starting with a cell of average size, $v_{target} = v_{target,average}$, causing it to grow at a constant rate until v_{target} increases to $2v_{target,average}$, and splitting the dividing cell into two cells, each with a new target volume: $v_{target}/2$. One daughter cell assumes a new identity (a unique value of σ). A breadth-first search selects the voxels which receive the new σ. The split is along a random, approximate cell diameter. The two halves are each connected.

4.2 Modeling Molecular Scales: Reaction-Diffusion Equations

Turing [33] introduced the idea that interactions of reacting and diffusing chemicals (usually of two species) could form self-organizing instabilities that provide the basis for biological spatial patterning (*e.g.*, to explain animal coat patterning, see [15] for a review). A slow-diffusing *activator* (*i.e.*, a chemical that has a positive feedback on its own production) and a fast-diffusing *inhibitor* can give rise to spatial patterns of high and low concentrations of activator. The key point is that the interaction of two processes (production and diffusion), can together destabilize a spatially homogeneous state. Various models have been proposed that RD mechanisms underlie the general features of chondrogenic patterning in the limb [3, 7] via morphogenetic signalling. We use this continuum PDE RD approach to model diffusible TGF-β in the limb domain. Such RD equations develop concentration patterns via the *Turing instability* mechanism.

We assume that diffusible morphogens diffuse in the mesoblast (consisting of ECM and cells) that fills the limb domain. Both cells and the ECM move within the limb domain, and the limb domain itself grows. We assume that advection effects are negligible since cell and ECM movement are much slower than diffusion.

Genetic programs cause cells to respond to threshold levels of TGF-β concentration (see Section 4.3), forming a spatial pattern that reflects the established pattern of TGF-β concentration. TGF-β thus forms the first *prepattern* which guides chondrogenic condensation.

In our *RD* model, the cells both produce and respond to the prepattern rather than simply following a laid-out prepattern [3]. This feedback affects the stability of patterns, often helping to *lock in* (stabilize) a pattern which would be transient without feedback. The production of the substrate molecule fibronectin (described in Section 4.3), forms the second *prepattern* for cell condensation which provides feedback and stability.

4.2.1 Reaction-Diffusion Continuum Submodels

The general form for RD equations is:

$$\frac{\partial u_i}{\partial t} = \sum_{j=1}^{n} d_j^i \frac{\partial^2 u_i}{\partial x_j^2} + \gamma F_i(u), \qquad (\mathbf{6})$$

Where $i=1,..,M$, $u=(u_1,..,u_M)^T$, u_i denotes the concentration of the ith chemical species, $F = (F_1,...,F_M)$: $\boldsymbol{R}^M \rightarrow \boldsymbol{R}^M$ is the reaction term and $\gamma > 0$ is an auxiliary parameter. Equation 6 applies to an open, bounded region $\Omega \in \boldsymbol{R}^n$, $n \geq 1$, with fixed or moving boundaries. $D = \{d_j^i\}_{j=1,...,n}^{i=1,...,M}$ is an $M \times n$ matrix of diffusion coefficients (with positive entries). We assume that the chemicals do not penetrate the boundary of Ω. The boundary conditions we use are no-flux:

$$\frac{\partial u_i}{\partial \hat{n}} = 0, \qquad (\mathbf{7})$$

where $\hat{n}$ is the unit outward normal to the boundary of Ω. The initial conditions are:

$$u(x,0) = u_{in}(x). \quad (8)$$

Often, as here, the number M of chemical species is 2. Conventionally, u_1 is an activator and u_2 an inhibitor.

For biological applications of RD see, amongst others, [6] and [15]. For simplicity, we assume isotropic diffusion, *i.e.*, d_j^i does not depend on j (we will later drop this restriction), so:

$$\frac{\partial u}{\partial t} = D\,\nabla^2 u + \gamma F(u), \quad (9)$$

where $u=(u_1,u_2)^T$ and $D = diag(d_1, d_2)$. Without loss of generality we can assume that:

$$d_1 = 1, d_2 = d. \quad (10)$$

For simplicity we also assume that Ω is a cuboid:

$$\Omega = (0, l_x) \times (0, l_y) \times (0, l_z). \quad (11)$$

Mathematically, the actions of activator and inhibitor mean that for a constant steady state u_0, we have $(\partial F_1/\partial u_1)>0$ if u_1 is an activator and $(\partial F_2/\partial u_2)<0$ if u_2 is an inhibitor. Commonly, we also assume that the inhibitor inhibits the activator and the activator activates the inhibitor ($(\partial F_1/\partial u_2)<0$ and $(\partial F_2/\partial u_1)>0$ respectively), but a bifurcation can also take place if the inhibitor activates the activator and the activator inhibits the inhibitor ($(\partial F_1/\partial u_2)>0$ and $(\partial F_2/\partial u_1)<0$)).

4.2.2 Turing Bifurcation

Let u_0 be a spatially uniform solution of $F(u)=0$ stable to spatially homogeneous perturbations. Grindrod [34] showed that u_0 is also a stable solution of Equation 9 if d is

small. A *Turing bifurcation* occurs when, at the *critical value* of $d = d_{crit}$ (for increasing, d, *i.e.*, an increasing diffusion rate), u_0 loses stability to a spatially varying stationary solution, generating a pattern [36]. This pattern first grows exponentially, but the nonlinear terms in the reaction kinetics F typically slow down the growth and eventually lead to a steady-state pattern. The wavelength of the final pattern need not correspond to the maximally unstable wavelength of the linearized equations.

The geometry of the RD domain also helps determine the pattern. If the domain size and pattern scale are comparable, the shape and exact size of the domain have a crucial influence on the pattern. A central idea in explaining the emergence of different patterns in the avian limb through Turing-type RD mechanisms relies on this dependence. Newman and Frisch [7] and Hentschel *et al*. [3] suggested that variations in the width of the Active Zone might produce the different patterns corresponding to the stylopod, zeugopod and autopod.

In addition, if the RD domain has certain spatial symmetries (for example a cube, sphere, or more generally, a rectangle whose edge ratios are integers), different *types* of pattern are possible. In a 2D square, these patterns are horizontal or vertical stripes, or spots. Ermentrout [35] has shown that stripes and spots cannot be simultaneously stable in this situation. Alber *et al.* [36] have generalized this result to 3D and higher dimensions. The nonlinear (quadratic and cubic) terms in the RD equations determine whether stripes or spots (or neither) are stable. Changing the nonlinear terms in F, can lead to a switch from stable spots to stable stripes or *vice versa*.

4.2.3 Application to Modeling the Avian Limb

Chaturvedi *et al.* [13] and Izaguirre *et al.* [14] used an *ad hoc* Schnakenberg form for F in Equation 9 for their 2D model of avian limb patterning [15]. The RD equations in this earlier model acted autonomously, providing a prepattern to which the cells responded. Here we use RD equations based on recent experiments on chondrogenesis in the early vertebrate limb and additional hypotheses which Hentschel *et al.* [3] developed in a 2D continuum context for the densities of different subtypes of mesenchymal cells and the activator-dependent production rates of activator and inhibitor. The activator and inhibitor is produced by the cells and thus depends on cell density, leading Hentschel and coworkers to term this a "reactor-diffusion" model [3]. This model reproduces the periodicity and stripe patterns of a centered longitudinal section of the real limb (2D case).

The RD equations based on [3] (corresponding to Equations 15 therein) thus become:

$$\begin{cases} \dfrac{\partial c_a}{\partial t} = \gamma[(J_0 + J_a(c_a)\beta(c_a))R_0 - k_a c_a c_i + K_a(c_a)R_0] + \\ \qquad (d_{ax}\dfrac{\partial^2 c_a}{\partial x^2} + d_{ay}\dfrac{\partial^2 c_a}{\partial y^2} + \dfrac{\partial^2 c_a}{\partial z^2}), \\ \dfrac{\partial c_i}{\partial t} = \gamma[J_i(c_a)\beta(c_a)R_0 - k_i c_a c_i + K_i(c_i)R_0] + \\ \qquad d(d_{ix}\dfrac{\partial^2 c_i}{\partial x^2} + d_{iy}\dfrac{\partial^2 c_i}{\partial y^2} + \dfrac{\partial^2 c_i}{\partial z^2}). \end{cases} \quad (\mathbf{12})$$

Here ds are diffusion coefficients and cs are concentrations of diffusing species. Subscript a denotes the activator, and subscript i the inhibitor. Subscript s denotes stable-state values. Subscripts x, y and z denote the spatial variation of the diffusion coefficients (equivalent to varying the limb cross-section as described below).

R_0 is the density of mobile cells in the continuum model [3]. Effectively, $\beta(c_a)$ denotes the fraction of R_o cells that produce the activator and inhibitor in Equations 12 through the mechanism of J_a and J_i. In [3], β corresponds to subtype R_2 of type R_0 (R_2 cells express FGF-2 receptor 1). The proportion $\beta(c_a)$ depends on the TGF-β concentration, c_a, due to simplifications of more complicated equations [3]. The crucial assumption which justifies the simplifications is that the overall mobile cell density changes slowly compared with the rate of cell differentiation. See [3] for more details and a biological discussion of the simplifications. Section 4.4 describes the various cell types, their characteristics, and their transition rules in more detail, and also discusses our implementation of R_0 and R_2 cells.

In Equation 12 we assume that the overall mobile cell density R_0 is constant, effectively decoupling the RD dynamics from the cell dynamics and simplifying computation. In the range of interest of R_0, the production of morphogens depends more on the rate constants and kinetic coefficients than on the cell density.

R_2 cells secrete TGF-β and inhibitor at activator-dependent rates $J_a(c_a)$ and $J_i(c_a)$, respectively. We use Hill kinetics [15] for these production rates [3]. The functional forms are:

$$\begin{cases} J_a(q) = \dfrac{8.0q^2}{6.25+q^2} \\ J_i(q) = \dfrac{8.6q^2}{6.25+q^2} \\ \beta(q) = \dfrac{0.745146q}{1.92248+q}. \end{cases} \quad \textbf{(13)}$$

The constant production rate J_0 of the activator is small compared to the term $J_a(c_a)\,\beta(c_a)$.

The cells also produce activator and inhibitor via the two terms, $K_a(c_a)R_0$ and $K_i(c_i)R_0$, on the right-hand side of Equations 12:

$$\begin{cases} K_a(c_a) = b_a(c_{as} - c_a)^3 \psi(c_a / c_{as}), & \text{and} \\ K_i(c_i) = b_i(c_{is} - c_i)^3 \psi(c_i / c_{is}) \end{cases} \quad . \tag{14}$$

Here $\psi(q)$ is a smooth step function with $\psi(q) = 1$ for q near 1 and $\psi(q) = 0$ for $q << 1$ and for $q >> 1$ and b_a and b_i are constants. ψ causes the terms $K_a(c_a)R_0$ and $K_i(c_i)R_0$ to operate only near the equilibrium concentration. These terms, which change the nonlinear (cubic) terms in the Taylor expansion of the reaction kinetics F, are necessary to guarantee that the proximo-distal cross-sections of the patterns are spot-like rather than stripe-like, resulting in cylindrical bones[7] (see also the discussion of the importance of nonlinear terms in Section 4.2.2 and references [35] and [36]). For studies of the effect of cubic terms on patterning in other physical models, including Rayleigh-Bénard convection and superconductivity, see [37], [38] and [39].

Due to the form of the terms $K_a(c_a)$ *and* $K_i(c_i)$, the terms with rates $J_a(c_a)$ and $J_i(c_a)$ dominate overall morphogen production both close to and far from equilibrium. $K_a(c_a)$ *and* $K_i(c_i)$ fine-tune the morphogen production rates to bias the emerging pattern to select spots rather than stripes in the proximo-distal cross sections while the concentrations are still close to equilibrium.

Pattern periodicity in RD depends on the solution domain. This dependence is biologically realistic: the antero-posterior width of the limb bud remains the same, but the

[7] We have effectively decoupled the RD prepattern (the first prepattern) from the cell dynamics by setting the cell density R_0 constant to the average cell density as a zeroth approximation to the interface between the CPM based cell dynamics and RD based activator and inhibitor dynamics. Including a further feedback mechanism from the cell to the RD prepattern, for example by computing instantaneous local cell density from the CPM might obviate the additional third-order terms $K_a(c_a)$ *and* $K_i(c_i)$. See the discussion of prepatterning mechanisms in the introduction to section 3.2

dorso-ventral thickness changes in the proximo-distal direction [7]. Changing spatial domains are numerically problematic. Here, we simplify this problem by using changing diffusion coefficients (Equations 12), which is equivalent to changing the aspect ratio of the domain [7]. If L is a constant length, then the transformation $x'=x/L$ leads to $\partial^2/\partial x'^2=L^2\ \partial^2/\partial x^2$, so the diffusion coefficient transforms as $d'=d/L^2$. For example, doubling one side length ($L=2$) is equivalent to dividing the corresponding diffusion coefficient by 2^2. Without loss of a generality, we set $d_{ax}=1$.

For a square domain, appropriately scaling the diffusion coefficients can produce different rectangular cross-sections in the forearm and digit areas.

We have numerically solved the full 3D Equations 12. The stable cylindrical structures resemble bone elements (see Figure 5 and Section 6). These structures provide a first template/prepattern, which coupled with the stabilizing feedback mechanisms at the cell level, result in chondrogenic patterning (Sections 4.3 and 4.4). We discretized Equations 12 using an explicit finite-difference scheme over rectangular domains. Space and time discretization relate through standard stability criteria. Separately, or in combination, the set of parameters γ, the ratio l_x/l_y and the diffusion coefficients of the activator and inhibitor equivalently control the number of cylindrical elements and their geometry.

4.3 Modeling Macromolecular Scales: Fibronectin Secretion

Our earlier 2D simulations assumed that cells move over a substrate coated with varying concentrations of non-diffusing fibronectin molecules [13, 14]. In 3D, we still assume that fibronectin remains at its secretion location and use a separate grid to track its

concentration. We could also model fibronectin on the CPM grid by making it into a generalized cell and adding appropriate CPM parameters like λ and J.

In our model, cells respond to the TGF-β chemical signal by producing fibronectin, and a cell-cell adhesion molecule (CAM) which we identify with N-cadherin. Cells, in turn, adhere to fibronectin-rich matrix and accumulate at points of highest concentration, because of their reduced mobility in this ECM microenvironment [8, 28, 29]. In addition, the fibronectin signal upregulates cell-cell adhesion, which enhances the accumulation of cells. Cells tend to cluster at high-fibronectin-concentration locations and reinforce this tendency by secreting more fibronectin.

Thus, although the Turing instability triggers patterning of fibronectin, self-enhancing, positive feedback, independent of TGF-β causes subsequent patterning. The fibronectin concentration pattern provides a prepattern for the cells. The model demonstrates global emergent phenomena resulting from local interactions.

4.4 Cell Types and the State-Transition Model

During morphogenesis, cells *differentiate* from initial multipotent stem cells into the specialized types of the developed organism. The concept of differentiation requires some discussion (see ref. [17]). Though every cell is different, identifying cells with broadly similar behaviors and grouping them as *differentiation types* is extremely convenient. Cell differentiation from one cell type to another is a comprehensive qualitative change in cell behavior, generally irreversible and abrupt (*e.g.*, responding to new sets of signals, turning on or off whole pathways). All cells of a particular differentiation type share a set of parameters describing their state, while two different cell types (*e.g.*, myoblasts and erythrocytes) have different parameter sets. Computationally, types are convenient but

not necessary. Cells of the same type can also exist in different *states*, corresponding to a specific set of values for the cell-type's parameter set. A cell's behavior depends on its state; two simulated cells behave identically in the same external environment if all parameters associated with their cell type are exactly the same, while cells of the same type with different parameter values can behave differently. Biologically, cells of the same type in different states typically differ less in their behavior than cells of two different types. Genetic and external cues influence both cells' type and state.

We model differentiation using a *type-change* map. Each type in this map corresponds to a cell type that exists during limb chondrogenesis. Change of a cell from one type to another corresponds to cell differentiation. The type-change map models regulatory networks by defining the rules governing type change, which accounts for the intra- and inter-cellular effects of chemical signals.

In the avian limb, the initial precartilage mesenchymal cells can translocate, divide, and produce various morphogens and ECM molecules. We assume that cells in the Active Zone represent a cell type distinct from those in the Apical Zone. Specifically, unlike the Apical Zone cells, Active Zone cells respond to activator, inhibitor, and fibronectin. They can also produce activator and inhibitor, and correspond to the R_0 type in Equations 12. Since β in Equations 12 implicitly accounts for the R_2 type, we do not include R_2 cells in the *type-change* map. When a responsive cell in the Active Zone senses a threshold local concentration of activator (TGF-β), its type changes to *fibronectin-producing*. A fibronectin-producing cell can upregulate its cell-cell adhesion (the parameter $J_{\tau\tau'}$ in the CPM decreases). Cells that have not experienced local threshold levels of activator can respond to, but not produce fibronectin. All cell types divide.

4.5 The Scale of the Organ: Integration of Submodels

The various biological mechanisms must work in a coordinated fashion. We therefore designed our computational environment to integrate the biological submodels while maintaining their modularity, *e.g.*, by:

1. Matching the spatial grid for RD and the CPM.
2. Defining the relative number of iterations for the RD and CPM evolvers.

The fibronectin and CAM submodels form a positive feedback loop (of fibronectin secretion and CAM upregulation) providing the *biologically-motivated* interface between the RD-based TGF-β prepattern and the CPM-based cell dynamics. TGF-β, the threshold concentration of which initiates differentiation (type change), provides the interface between RD and the type-change map. The type-change map chooses parameter sets and their parameters in the CPM representation.

4.6 Environment Implementation: Modular Framework and Integration

The front and back ends of the environment are distinct modules. The back-end consists of two engines that carry out most calculations—a computational engine, which combines the various biological submodels, and a visualization engine for graphics that can run independently. The front end to the engines provides a file-based user-interface for simulation parameters and visual display. The computational engine has three main modules: the CPM engine (stochastic, discrete), the Reaction-Diffusion engine (continuum, PDEs), and the type-change engine (a rule-based state automaton).

The RD engine uses an explicit solver, based on forward time marching. We store these calculations as *fields*, *e.g.,* the fibronectin concentration. The CPM simulator implements the lattice abstraction and the Monte Carlo procedure. The acceptance

probability function is Metropolis. We can view the CPM as an operation on a field of voxels. Various fields can evolve under their own set of rules—Metropolis dynamics for the field of voxels, RD for the field of morphogens. A chemical like fibronectin, which cells secrete and which then remains in place is another concentration field, with a reaction dynamics with no diffusion. A version of this environment, *CompuCell3D*[8], is available for download. For the detailed design of the computational environment see [47].

In order to integrate these modules, we specify criteria for interpolating between the various grids and the order in which to evolve fields.

Other sub-modules implement different cell responses, *e.g.*, cell growth and mitosis.

We used the Visualization ToolKit (VTK), available as freeware[9] to develop our visualization software.

5 Discussion of Simulation Results

How do parameters affect the integrated model? We start with an initial distribution of undifferentiated cells in the ECM, with a cell-volume less than the average cell volume (Table 1), no initial fibronectin and a small, randomly perturbed, distribution of activator and inhibitor. The combination of morphogens, cell dynamics and cell differentiation produces the roughly periodic pattern of the major chondrogenic elements in the chick limb. Table 2 lists the important mechanisms and the corresponding control parameters, to emphasize that although the integrated model has a large number of parameters, only a few specific parameters control each mechanism.

[8] http://www.nd.edu/~lcls/compucell
[9] http://public.kitware.com/VTK/get-software.php

We first present a parameter set for normal patterning of chick forelimb precartilage condensation: one followed by two and then three primary parallel skeletal elements successively in the distal direction. Figure 5 shows a time series (in the growing distal direction) for the activator concentration during "first" prepattern formation. Cells exposed to an above-threshold activator concentration begin and continue to secrete fibronectin. In response to fibronectin, cells undergo haptotaxis and become more adhesive to each other so the fibronectin concentration ("second" prepattern) and cell-condensation (skeletal elements) pattern follow the activator prepattern.

Fibronectin produces a positive feedback loop that stabilizes cell condensations. Figure 6 shows the distribution of fibronectin in the limb at different times. The fibronectin pattern forms relatively quickly (about 20 times faster than the final cell condensations, see Figure 6 and its caption). Figure 7 shows simulations of the full 3D chick-limb chondrogenesis model, where the cells have condensed into the chondrogenic pattern of a chick forelimb. Table 3 gives the complete set of parameter values for these simulations. Parameters specific to the RD part of the model with cubic terms correspond to Equations 12.

We next study parameter sets resulting in two cases of abnormal development.

Figure 8 shows a case where four rather than three digits form, corresponding to polydactyly. All parameters are the same as in normal development (Table 3), except that the transition of d_{ax}=d_{ix} to the value of 1/12 occurs later than normal, *e.g.*, due to abnormal FGF signaling and/or late response of the cells secreting morphogens at the proximal boundary of the Apical Zone. Figure 9 (a) displays the fibronectin distribution and 9 (b) the resulting cell condensations.

Figure 10 shows a case of fused skeletal elements, corresponding in certain respects to the pathology of the human genetic condition known as Apert's syndrome [42]. Figure 10 (a) shows the TGF-β ("first") prepattern along the distally growing limb bud. In the proximal region, the one-cylinder pattern (one spot in transverse section) is stable, followed by a bifurcation of the solution into two cylindrical elements (two spots in cross-section). The two elements then fuse into one long stripe in the transverse section. Figure 10 (b) displays the corresponding fibronectin pattern. We obtained this pathology by setting d_{ax}=d_{ix}=1/14 in the digits (the three-skeletal-element region) instead of 1/12 (see Table 3), and having the transitions in d_{ax} and d_{ix} occur later than normal, *e.g.*, due to an abnormal limb-cross-section aspect ratio or abnormal FGF signaling.

The two pathological cases suggest that domain-size changes in the Apical and Active Zones, which we implemented *a priori*, affect the location and periodicity of skeletal element condensations. A fuller model would include FGF signaling from the AER to control the evolution of the Apical and Active Zones, and morphogen control of dorso-ventral and antero-posterior geometry.

Work in progress: We are enhancing the realism of this class of models to include the complex geometry of the limb bud. We are also incorporating the effects of factors (*e.g.*, Wnt-7A, Gli3 and Sonic hedgehog) that control limb geometry and zones.

Acknowledgements: We acknowledge support from NSF Grants IBN-0083653 and ACI-0135195, NASA grant NAG 2-1619, the IUB Pervasive Technologies Laboratories and an IBM Innovation Institute Award.

References

[1] J. A. Glazier, F. Graner, F., A simulation of the differential adhesion driven rearrangement of biological cells, Phys. Rev. E 47 (1993) 2128-2154.

[2] F. Graner, J. A. Glazier, J. A., Simulation of biological cell sorting using a 2Dimensional extended Potts model. Phys. Rev. Lett. 69 (1992) 2013-2016.

[3] H. G. E. Hentschel, T. Glimm, J. A. Glazier, S. A. Newman, Dynamical mechanisms for skeletal pattern formation in the vertebrate limb. Proc. R. Soc. Lond: Bio. Sciences **271** (2004) 1713-1722.

[4] Y. Jiang, H. Levine, J. A. Glazier, Possible cooperation of differential adhesion and chemotaxis in mound formation of Dictyostelium. Biophys. J. 75 (1998) 2615-2625.

[5] M. Kiskowski, M. Alber, G. L. Thomas, J. A. Glazier, N. B. Bronstein, J. Pu, S. A. Newman, Interplay between activator-inhibitor coupling and cell-matrix adhesion in a cellular automaton model for chondrogenic patterning. Dev. Biol. 271 (2004), 372-387.

[6] H. Meinhardt, Models of Biological Pattern Formation, Academic Press, London, 1982.

[7] S. A. Newman, H. L. Frisch, Dynamics of skeletal pattern formation in developing chick limb, Science 205 (1979) 662-668.

[8] W. Zeng, G. L. Thomas, S. A. Newman, J. A. Glazier, A Novel Mechanism for Mesenchymal Condensation during Limb Chondrogenesis in vitro, in Mathematical Modeling and Computing in Biology and Medicine: 5th Conference of the European Society of Mathematical and Theoretical Biology, Milan, V. Capasso and M. Ortisi (ed.) (2002).

[9] A. F. M. Marée, P. Hogeweg. How amoeboids self-organize into a fruiting body: multicellular coordination in *Dictyostelium discoideum*, in Proc. Natl. Acad. Sci. U.S.A. (2001) 98:3879-3883.

[10] A. F. M. Marée, P. Hogeweg. Modelling *Dictyostelium discoideum* morphogenesis: the culmination, Bull. Math. Biol. (2002) 64:327-353.

[11] M. Kerszberg, J.-P. Changeux, A simple model of neurulation, Bioessay 20 (1998) 758-770.

[12] M. Zajac, G. L. Jones, J. A. Glazier, Simulating convergent extension by way of anisotropic differential adhesion, J. Theoret. Bio. (2003) 222/2, 247-59.

[13] R. Chaturvedi, J. A. Izaguirre, C. Huang, T. Cickovski, P. Virtue, G. Thomas, G. Forgacs, M. Alber, G. Hentschel, S. A. Newman, J. A. Glazier, Multi-model simulations of chicken limb morphogenesis, in Computational Science – ICCS 2003: International Conference Melbourne, Australia and St. Petersburg, Russia, June 2-4, 2003. Proceedings, Part III, P. M. A. Sloot, D. Abramson, A. V. Bogdanov, J. J. Dongarra, A. Y. Zomaya and Y. E. Gorbachev editors (Lecture Notes in Computer Science 2659, Springer Verlag, New York, 2003), 39-49.

[14] J. A. Izaguirre, R. Chaturvedi, C. Huang, T. Cickovski, J. Coffland, G. Thomas, G. Forgacs, M. Alber, G. Hentschel, S. A. Newman, J. A. Glazier, CompuCell, a multi-model framework for simulation of morphogenesis, Bioinformatics 20 (2004) 1129-1137.

[15] Murray, J.D., Mathematical Biology, Springer, Berlin, 2nd edition, 1993.

[16] S. A. Newman, W. D. Comper, 'Generic' physical mechanisms of morphogenesis and pattern formation, Development 110 (1990) 1-18.

Formatted: German (Germany)

Formatted: German (Germany)

[17] S. A. Newman, G. Forgacs, Complexity and self-organization in biological development and evolution, in Complexity in Chemistry, Biology, and Ecology, eds. Bonchev, D. and Rouvray, D. H. Springer, New York, in press.

[18] S. A. Newman, Lineage and pattern in the developing vertebrate limb, Trends in Genetics 4 (1988) 329-332.

[19] M. S. Steinberg, Goal-directedness in embryonic development, Integrative Biology 1 (1998) 49-59.

[20] C. M. Leonard, H. M. Fuld, D. A. Frenz, S. A. Downie, J. Massague, S. A. Newman, Role of transforming growth factor-β in chondrogenic pattern formation in the embryonic limb: stimulation of mesenchymal condensation and fibronectin gene expression by exogenenous TGF-β and evidence for endogenous TGF-β like activity, Dev. Biol. 145 (1991) 99-109.

[21] P. A. Tsonis, K. Del Rio-Tsonis, J. L. Millan, M. J. Wheelock, Expression of N-cadherin and alkaline phosphatase in the chick limb bud mesenchymal cells: Regulation by 1,25- dihydroxyvitamin D_3 and TGF-β1, Exp. Cell Res. 213 (1994) 433- 437.

[22] K. Del Rio-Tsonis, P. A. Tsonis, Expression of transforming growth factor-â 1-4 in the chick limb bud mesenchymal cells: Regulation by 1,25 dihydroxyvitamin D_3, Biochem. Biophys. Res. Commun. 204 (1994) 975-982.

[23] E. Van Obberghen-Schilling, N. S. Roche, K. C. Flanders, M. B. Sporn, A. B. Roberts, Transforming growth factor β 1 positively regulates its own expression in normal and transformed cells, J. Biol. Chem. Vol. 263 Issue 16 (Jun 1988) 7741-7746.

[24] T. Miura, K. Shiota, TGF β2 acts as an activator molecule in reaction-diffusion model and is involved in cell sorting phenomenon in mouse limb micromass culture, Dev. Dyn. 217 (2000) 241-249.

[25] T. Miura, K. Shiota, The extracellular matrix environment influences chondrogenic pattern formation in limb micromass culture: experimental verification of theoretical models of morphogenesis, Anat. Rec. 258 (2000) 100-107.

[26] T. Miura, M. Komori, and K. Shiota, A novel method for analysis of the periodicity of chondrogenic patterns in limb bud cell culture: correlation of in vitro pattern formation with theoretical models, (2000) Anat. Embryol. (Berl.) 201, 419-428.

[27] M. Z. Moftah, S. Downie, N. Bronstein, N. Mezentseva, J. Pu, P. Maher, S. A, Newman, Ectodermal FGFs induce perinodular inhibition of limb chondrogenesis in vitro and in vivo via FGF receptor 2, Dev. Biol. 249 (2002) 270-282.

[28] D. A. Frenz, N. S. Jaikaria, S. A. Newman, The mechanism of precartilage mesenchymal condensation: a major role for interaction of the cell surface with the amino-terminal heparin-binding domain of fibronectin, Dev. Biol. 136 (1989) 97-103.

[29] D. A. Frenz, S. K. Akiyama, D. F. Paulsen, S. A. and Newman, Latex beads as probes of cell surface-extracellular matrix interactions during chondrogenesis: evidence for a role for amino-terminal heparin-binding domain of fibronectin, Dev. Biol. 136 (1989) 87-96.

[30] J. H. Lewis, Fate maps and the pattern of cell division: a calculation for the chick wing-bud, J. Embryol. Exp. Morphol. 33 (1975) 419-34.

[31] M. S. Steinberg, Reconstruction of tissues by dissociated cells, Science 141 (1963) 401-408.

[32] A. Upadhyaya, Thermodynamic and fluid properties of cells, tissues and membranes, Ph.D. thesis, University of Notre Dame, 2000.

[33] A. Turing, The chemical basis of morphogenesis, Phil. Trans. Roy. Soc. Lond. B 237 (1952) 37-72.

[34] P. Grindrod, Patterns and waves, Clarendon Press, Oxford, 1991.

[35] B. Ermentrout, Stripes or spots? nonlinear effects in bifurcation of reaction-diffusion equations on the Square, Proc. R. Soc. Lond. A 434 (1991), 381-417.

[36] M. Alber, T. Glimm, H. G. E. Hentschel, B. Kazmierczak, S. A. Newman, Stability of n-Dimensional Patterns in a Generalized Turing System: Implications for Biological Pattern Formation, Nonlinearity (2004) (to appear).

[37] J. Swift, P. C. Hohenberg, Hydrodynamic fluctuations at the convective instability, Physical Review A 15 (1) (1977) 319-328.

[38] E. Bodenschatz, W. Pesch, G. Ahlers, Recent developments in Rayleigh-Benard convection, Annu. Rev. Fluid Mech. 2000 32 (2000) 709–778.

[39] V. L. Ginzburg, L. D. Landau, On the theory of superconductors, Soviet Phys. JETP, 20 (1950), 1064. (Ginzburg, V. L. and Landau, L. D., Zh. Eksp. Teor. Fiz. 20 (1950) 1064).

[40] S. A. Downie, S. A. Newman, Different roles for fibronectin in the generation of fore and hind limb precartilage condensations. Dev. Biol. 172 (1995) 519-530.

[41] A. L. Gehris, E. Stringa, J. Spina, M. E. Desmond, R. S. Tuan, V. D. Bennett, The region encoded by the alternatively spliced exon IIIA in mesenchymal fibronectin appears essential for chondrogenesis at the level of cellular condensation. Dev Biol 190 (1997) 191-205.

[42] I. Wierzbicka-Patynowski, J. E. Schwarzbauer, The ins and outs of fibronectin matrix assembly, Journal of Cell Science 116 (2003) 3269-3276.

[43] M. M. Cohen, Jr., S. Kreiborg, Hands and feet in the Apert syndrome, Am J Med Genet 57 (1995) 82-96.

[44] R. Chaturvedi, C. Huang, J. A. Izaguirre, S. A. Newman, J. A. Glazier, M. Alber, A hybrid discrete-continuum model for 3D skeletogenesis of vertebrate limb, *accepted for publication in* Lecture Notes in Computer Science, Springer-Verlag, New York (Proceedings of ACRI 2004, From Individual to Collective Behaviour).

[45] B. K. Hall, T. Miyake, All for one and one for all: condensations and the initiations of skeletal development, Bioessays, 22.2, (2000), 138-147.

[46] N. B. Ouchi, J. A. Glazier, J. Rieu, A. Upadhyaya, Y. Sawada, Improving the realism of cellular Potts model in simulations of biological cells, Physica A (329) (2003) 451-458.

[47] T. Cickovski, C. Huang, R. Chaturvedi, T. Glimm, H.G.E. Hentschel, M. Alber, J. A. Glazier, S. A. Newman, J. A. Izaguirre, A Framework for Three-Dimensional Simulation of Morphogenesis, submitted, IEEE/ACM Transactions on Computational Biology and Bioinformatics, 2004 (submitted for publication).

Figures and Tables

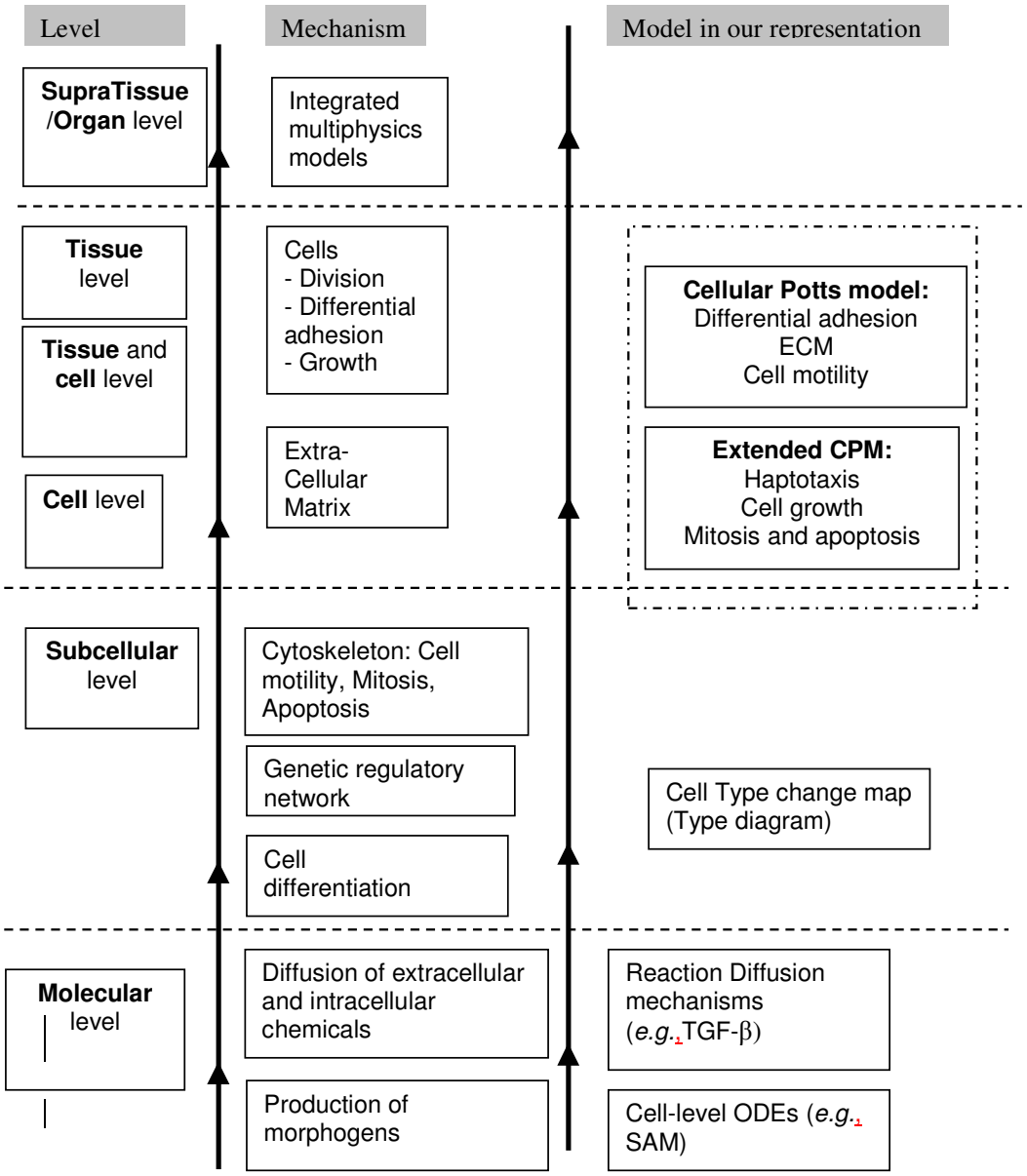

Figure 1: Hierarchy of scales from molecule to organ, and the corresponding mechanisms and modeling approaches. Models/subsystems at coarser scales use information from finer scales.

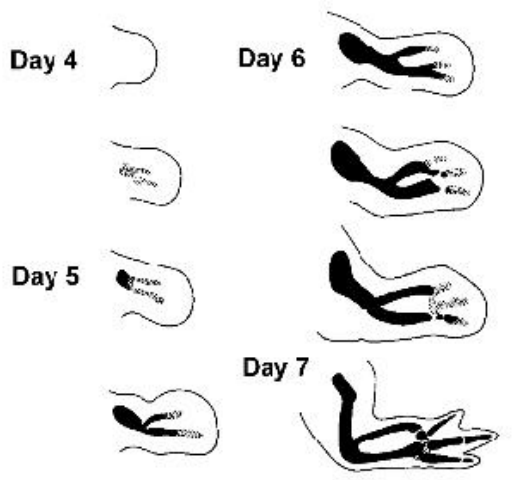

Figure 2: Skeletal pattern formation: Time-series of chick limb-bud development in longitudinal section. For each figure, proximal is to the left, distal to the right, anterior up and posterior down. Black represents differentiated cartialge and stipple precartilage condensation. (Based on [7]).

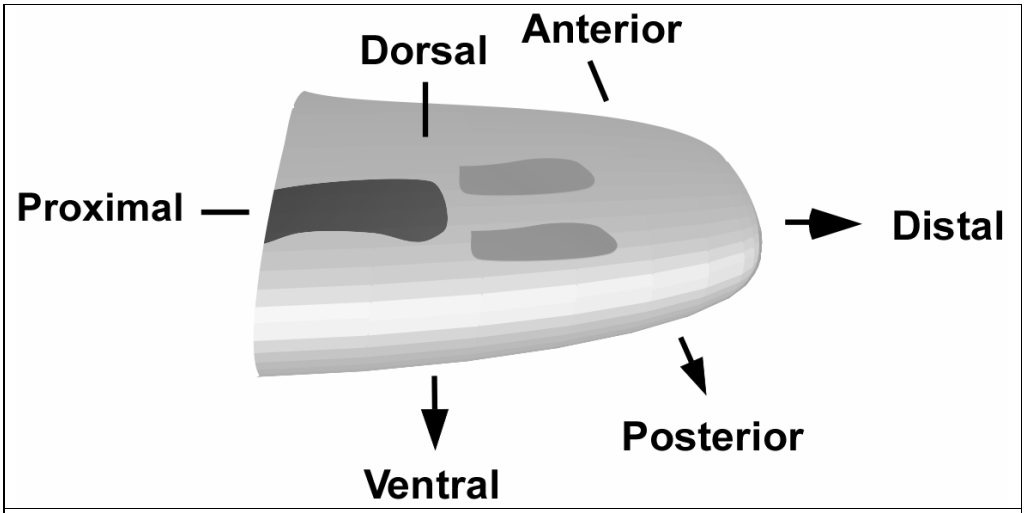

Figure 3: Schematic diagram of chick limb organogenesis at mid-development (correponding to day 5 in Fig. 2), showing primary axes. The earliest-developing region of the skeleton has differentiated into cartilage (black) by this stage. The region in which skeletal pattern is newly-forming is undergoing mesenchymal condensation (medium gray). The digits at the distal region have not yet begun to form.

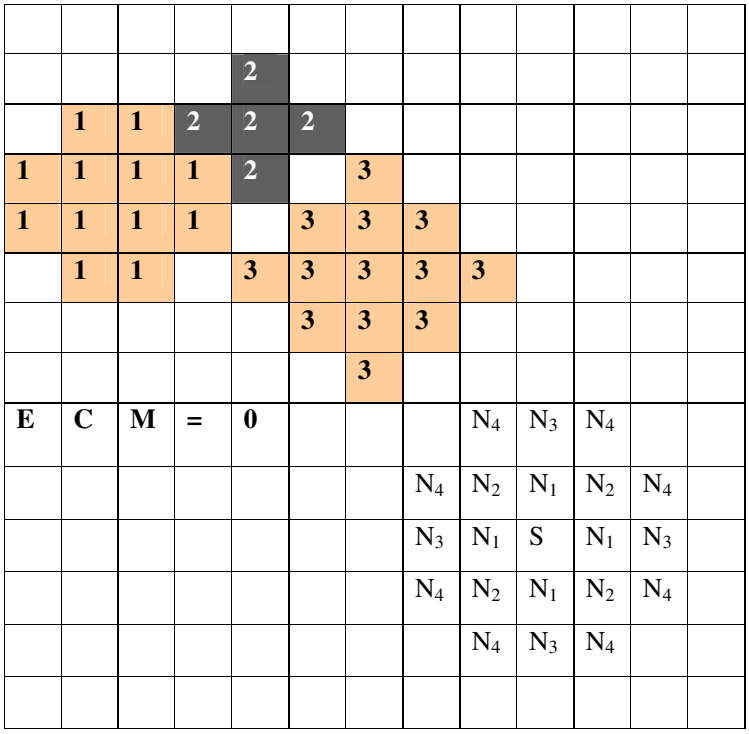

Figure 4: The CPM grid and representation of cells and ECM. The shading denotes the cell type. Different cells (*e.g.*, cells 1 and 3) may have the same cell type. We also show the fourth-neighbor interactions of voxel S on a 2D grid.

Figure 5: Time-series of the concentration of the diffusible morphogen TGF-β for Equations 12 (displayed along proximo-distal cross sections) with time increasing along the distal direction (upwards). This "first" prepattern of cylindrically elongated parallel elements drives "final" cell condensation through the mediating "second" prepattern of non-diffusing fibronectin. Proximal direction is denoted by "p", ventral by "v" and anterior by "a".

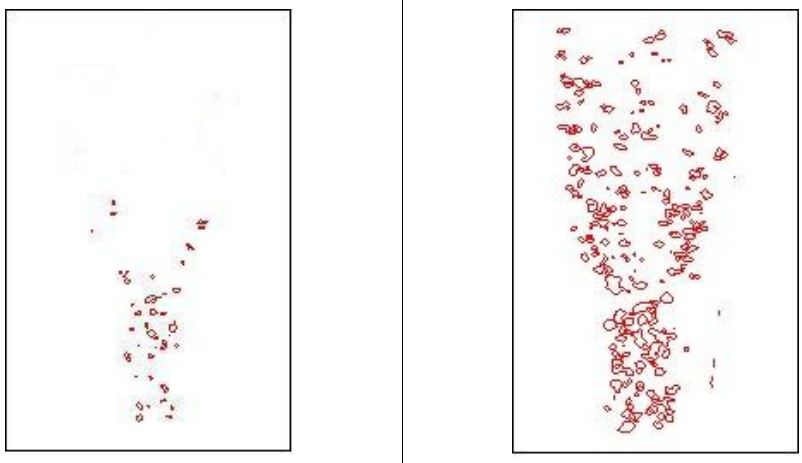

(a) (b)

Figure 6: Fibronectin production corresponding to normal chondrogenesis. Fibronectin accumulation is shown along distal direction, as time progresses and the limb grows. Haptotaxis of cells in response to fibronectin ("second" prepattern), and cells' continuing fibronectin secretion, makes the patterning robust and does not require a persistent activator ("first") prepattern. The fibronectin pattern establishes itself faster (a) 400 Monte Carlo steps (half-formed limb) (b) 800 Monte Carlo steps (fully-formed limb) than the final cell condensations (1040 Monte Carlo steps, Figure 7), emphasizing fibronectin's role in pattern consolidation. Fibronectin accumulates at its secretion location: its concentration in the humerus region in (b) is larger than in (a).

	Figure 7: Cell condensation into humerus, ulna+radius, and digits after 1040 Monte Carlo steps. Visualization is done using volume rendering. The axes correspond to “p”, “a” and “v” of Figure 5.

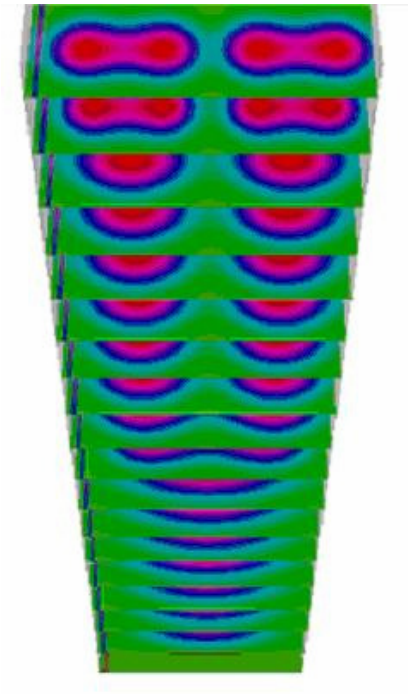

Figure 8: Time series (successive transverse cross-sections in the distal direction) of TGF-β concentration in a growing limb bud, corresponding to the pathology of extra digits (4 digits form instead of 3, see Figure 9).

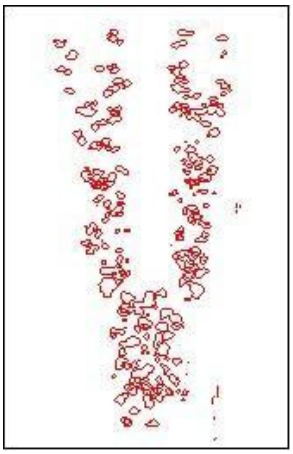

(a)

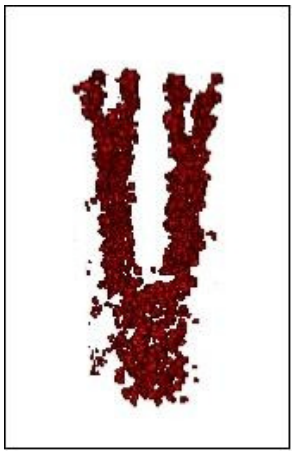

(b)

Figure 9: (a) Fibronectin distribution and (b) cell condensation, after 940 Monte Carlo steps, corresponding to the TGF-β (“first”) prepattern in Figure 8.

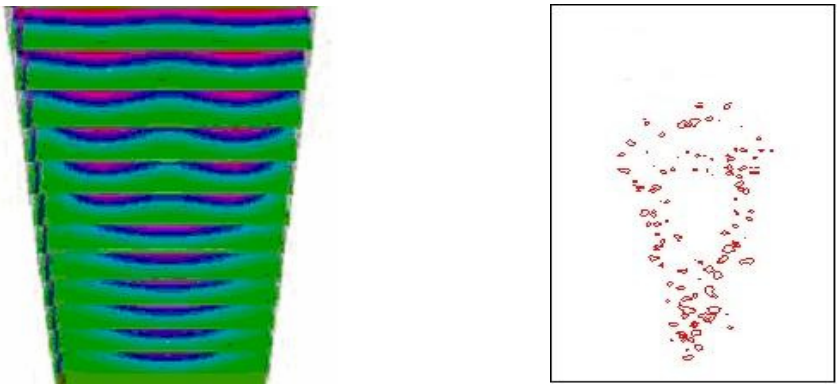

(a) (b)

Figure 10: (a) Time series (successive transverse cross-sections in the distal direction) of the TGF-β concentration in a growing limb bud, corresponding to the pathology of Apert's syndrome. (b) The fibronectin concentration field after 500 Monte Carlo steps (limb not fully formed). The radius and ulna fuse and digits fail to form.

Table 1: Summary of multiscale models.

S. No.	Mechanism	Modeling approach
1	Dynamics of morphogen fields	Activator, TGF-β and inhibitor interacting via reaction-diffusion partial differential equations
2	Establishment of fibronectin field	A grid to accumulate fibronectin secreted by cells, modeled using the Cellular Potts Model
3	Upregulation of cell-cell adhesivity	Individual cell's gene network modeled using ordinary differential equations
4	Dynamics of cells and their response to morphogen fields	Cellular Potts Model
5	Mitosis	An *ad hoc* approach based on a breadth first search incorporated into CompuCell 3.
6	Geometry of the limb space	Simplified into a 3D cuboidal domain
7	Definition of subzones in the spatial domain in which mechanisms 1-5 are active	Division of discretized space into zones
8	Mechanism to stop activator and cell evolution once the desired patterns have formed	Based on visualization and observation of numerical experiments

Table 2: Specific roles of important parameters.

	Phenomenon	Governing parameter	Equation/ Section
1.	Cell clustering	$J_{\tau,\tau'}$	1st term in Equation 2, detailed in Equation 3 (CPM)
2.	Limb prepatterning and patterning	Can equivalently use one of the following: D_x/D_y, γ	RD system Equations 15 and 16
3.	Haptotaxis	$\mu(\vec{\sigma})$	Equation 5
4.	Cell volume	λ_σ and v_{target}	Equation 4
5.	Cell growth leading to mitosis	v_{target} as a function of time	Equation 5
6.	Membrane fluctuations	T	Equation 1 Boltzmann Dynamics in CPM

Table 3: Values of parameters for normal limb simulations.

RD equations with stabilizing cubic terms	
Domain Length	2π
Domain Width	$6\pi/7$
γ	100.0 (humerus region), 180.0 (radius+ulna), 1710.0 (digits)
J_0	*0.04*
k_a	*1.0*
k_i	*1.0*
R_0	*2.0*
D	5.0
$d_{ax} = d_{ix}$	1.0 in humerus (1 skeletal element) region 1/4 in radius + ulna (2 skeletal elements) region 1/12 in digits (3 skeletal elements) region
$d_{ay} = d_{iy}$	0.15
$b_a/(\gamma R_0)$	0.02
$b_i/(\gamma R_0)$	-0.6
c_{as}	1.32494
c_{is}	0.86545
Δx	$\pi/35$
Δt	0.00002

CPM parameters	
Fluctuation temperature T	1.5
J (non condensing)	7.0
J (condensing)	Up to 0.5
Volume param., λ_σ	3.0
Target volume, v_{target}	16 voxels, grows to 32 voxels before mitosis
Surface param., λ_σ	Not used (Ø)
Haptotaxis param., μ	50.0

Fibronectin parameters	
Fibronectin production rate	0.15 per time step
TGF-β threshold	0.15

Integration, Grid and Numerics Parameters	
Domain Discretization	Number of subdivisions in (X,Y,Z) = (71,31,211), corresponds to dorso-ventral: antero-posterior: proximo-distal = 1: 2.3:6.8. A rectangular approximation to a typical limb bud is X=3.1mm, Y=1.6 mm, final Z length after growth=10.8mm (1.9:1:6.8). Same grid size used for CPM and RD.
Time steps	100 RD steps per CPM step, 71x31x211 trials per CPM step
Total time	Day 4 to day 7 (total of 3 days) covering stages 20 to 30 of chick limb growth. Total time steps = 300 CPM steps